J Mater Sci (2011) 46:7401–7409
DOI 10.1007/s10853-011-5702-6

Surface form memory by indentation and planarization of NiTi: displacements and mechanical energy density during constrained recovery

Xueling Fei · Corey J. O'Connell · D. S. Grummon · Yang-Tse Cheng

Received: 13 April 2011 / Accepted: 7 June 2011 / Published online: 8 July 2011

Abstract Indentation-induced two-way shape memory leads to pronounced temperature dependence of the depth of spherical indents made in martensitic NiTi shape-memory alloys. They are shallower when austenitic, and depth varies during both M → A and A → M transformations. If the impression is planarized, by metallographic grinding at $T < M_f$, a *protrusion* rises at the site when warmed past A_f. If cooled again this "exdent" retreats, restoring optical flatness. The cycle is repeatable, and exdent heights can exceed 15% of prior indent depth. Since it maps between macroscopically distinguishable topographies, or forms, at orders greater length scale than the surface roughness, we call the effect "surface form memory"—SFM. Notable regarding potential applications is that, when loaded in compression by planar contact with a strong base metal, exdents exert sufficient pressure to indent the latter, suggesting that subsurface transformational mechanisms operate at volumetric work-energy densities $>10^7$ J/m^3, fully ~10% of the M → A enthalpy.

Introduction

Shape memory in metal alloys is usually exploited to produce thermally driven axial displacements in wires, or isothermally recoverable bending strains in more complex shapes [1–5]. The technological significance of NiTi alloys in these contexts is that work- or stored-energy densities exceeding ten million joules per cubic meter may be obtained from well-designed actuators and flexures [6]. Furthermore, various thermomechanical processing strategies have been developed that allow for cyclic thermal displacements, involving a memory of both warm and cool shapes [7–9].

We have recently shown [10, 11] that the shape memory effect can be harnessed to produce marked, non-trivial, cyclically repeatable and, most importantly, *engineered* changes in overall surface topography, at the length-scale of the surface *form* (i.e., at a much greater scale than the intrinsic surface roughness). The mechanisms exploited to create this effect are essentially the same as those underlying changes in surface roughness often observed during metallographic preparation of Nitinol specimens. In this study, however, using a technique involving spherical or cylindrical indentation, followed by global surface planarization (accomplished by flat grinding), we have been able to prepare surfaces that exhibit radical changes in surface form, for example, between optical flatness and pronounced bumpiness or waviness. We call the effect surface form memory (SFM). An example of an SFM transition involving a single cylindrical indent is shown in Fig. 1. As we furthermore demonstrate in this article, the out-of-plane displacements that are observed in SFM can actually indent other materials. We show that NiTi alloys with surfaces prepared to exhibit SFM can perform mechanical work with sufficient energy to induce localized plastic deformation in a strong base metal substrate such as 304 stainless steel (SS).

The ability of SFM to generate transitions in surface form that can be normalized to a planar reference state, and do so against very high reaction forces, suggest that the effect could find application to MEMS actuators, lithography,

X. Fei · C. J. O'Connell · D. S. Grummon (✉)
Department of Chemical Engineering and Materials Science, Michigan State University, East Lansing, MI 48824, USA
e-mail: grummon@egr.msu.edu

Y.-T. Cheng
Department of Chemical and Materials Engineering, University of Kentucky, Lexington, KY 40506, USA

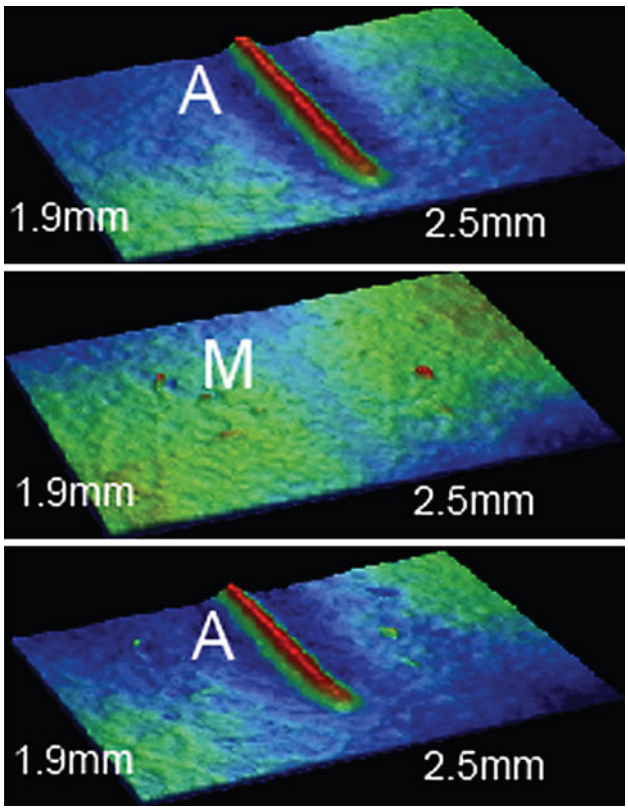

Fig. 1 Surface form memory transition enabled by cylindrical indentation followed by thermal cycling and planarization in the martensitic condition. The z-axis scale is magnified: the actual height of the exdent in this 1.9 × 2.5 mm field is about five microns

joining, mold-release, tribological systems, microassembly, electrical switching, variable heat transfer devices, and so on. Furthermore, the effect may be readily induced both macroscopically, and at the nanoscale [11], suggesting the possibility that SFM could enable optical applications such as thermally switchable diffraction gratings. The effect may be obtained either from indents made quasistatically, or by indenting in the dynamical regime using shocks from laser ablation [12]. Finally, the technique can be adapted to produce surface forms that map to complex indenter geometries, such as engraved images.

Shallow spherical indents made in martensitic NiTi will revert to near-perfect flatness, via the shape memory effect, when first heated past A_f [13]. However, deeper spherical[1] indents do not "recover" completely. The limit for full recovery, for the spherical case, can be expressed in terms of the ratio of the (in-plane) indent radius, a, to the radius, r, of the indenter itself. The a/r ratio determines the representative strain, ε_r, produced by indentation, which in turn correlates with the plastic component of the total strain in tensile tests [14, 15]. For spherical indentation, ε_r can be shown to equal 0.2 a/r [14]. For cylindrical indenters, the ratio of the indent half-width to the cylinder radius, c/r determines the representative strain via a different functional relationship.

When spherical indents are made in martensitic NiTi with a/r exceeding 0.25, such that ε_r exceeds a critical value of 5%, not only does the indent fail to recover fully on austenitization, but subsequent thermal cycling between M_f and A_f reveals that a two-way shape memory effect (TWSME) occurs at and just beneath the surface. In this case, thermal cycling causes the indent to be relatively deep when cool, but to become shallower when warmed past A_f. It is almost certainly not coincidental that the 5% limiting strain for this two-way effect corresponds approximately to the end of the detwinning plateau in tensile deformation of martensitic NiTi [13], and thus to the onset of the generation of dislocations in the martensite phase.

Figure 2 illustrates schematically the sequence of spherical indentation (a, b), indent recovery via TWSME (b, c), planarization (d), and cyclic exdent formation and retreat (d, e). Indentation with a ball of radius r, to a depth h, such that the resultant a/r ratio exceeds 0.25, results in cyclic displacement δ_1 on subsequent thermal cycling. If the indent is removed by flat grinding, further thermal cycling produces a cyclic displacement, δ_2, for the exdent. The displacements δ_1 and δ_2 are generally nearly equal, indicating that the material laterally adjacent to the indent (the material removed by planarization) does not contribute significantly to the two-way strain.

It is thus apparent that two-way displacements depend on deformation zones lying beneath the base of the indent. In Fig. 2b, three notional deformation zones are schematically indicated. Farthest from the indent is zone C, an elastic deformation zone bounded approximately by the 1% strain contour. Zone B is a region in which plasticity has occurred, but only via martensite detwinning reactions that are thermally reversible via the shape memory effect. The upper boundary of this zone corresponds to a strain contour at 5–7%, the approximate limit for one-way shape memory, i.e., roughly coincident with the end of the plateau in the martensite tensile stress–strain curve.

Heating after indentation will cause recovery of all of the strain in zone B, by an one-shot shape memory effect, but no further active transformational displacements will occur in this zone on subsequent cooling. On the other hand, in zone A, the local plastic strain has exceeded that which can be mediated by detwinning reactions, requiring the generation of geometrically necessary lattice dislocations. It is in this zone that two-way shape memory originates, with martensite variants reflecting the cool shape

[1] Conical indenters, such as Berkovitch, Knoop, or Vickers indenters, do not fully recover unless the depth of penetration is so small that natural blunting of the otherwise sharp tip makes it appear to the medium as spherical.

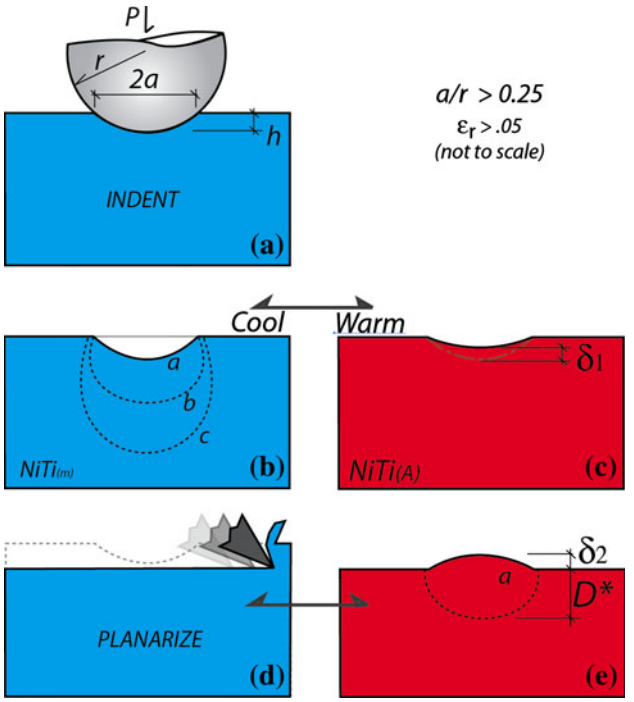

Fig. 2 Indent training (**a**–**c**) and planarization (**d**) to obtain SFM in NiTi. Thermally cycling between **b** ⇔ **c** and between **d** ⇔ **e** is indefinitely repeatable. Indentation results in three deformation zones under the indent: *a* plastic slip zone, *b* detwinned martensite zone, *c* elastic deformation zone

having been stabilized by the stress fields associated with the dislocations that now reside in this zone. For shallow indents (with $a/r < 0.25$, and thus, $\varepsilon_r < 5\%$) the volume of material in zone A is negligible, and the two-way effect is absent. We therefore associate the boundary between zones A and B with the spatial extent of the subsurface deformation zone that is responsible for SFM effects. If it is assumed that this zone is roughly hemispherical, its volume can be characterized by a single parameter, D^*, the depth of the zone A/zone B boundary, referred to the base of the original indent. The volume of the active zone is then approximated as $2/3\pi D^{*3}$.

We have made indirect experimental measurements of D^* over a range of a/r ratios [12, 16]. This was accomplished by successive planarization experiments in which material was incrementally removed from the surface until the cyclic recovery displacement δ_1 was observed to vanish. These measurements were confirmed by back thinning experiments in which material is removed from the surface opposite to the indent, again in a series of steps, until the magnitude of δ_1 just began to decline. Both methods generated similar results.

In this article, we show that an exdent features formed in an SFM cycle can exert very appreciable levels of force when the out-of-plane displacement is mechanically constrained. We present the results of constrained-recovery

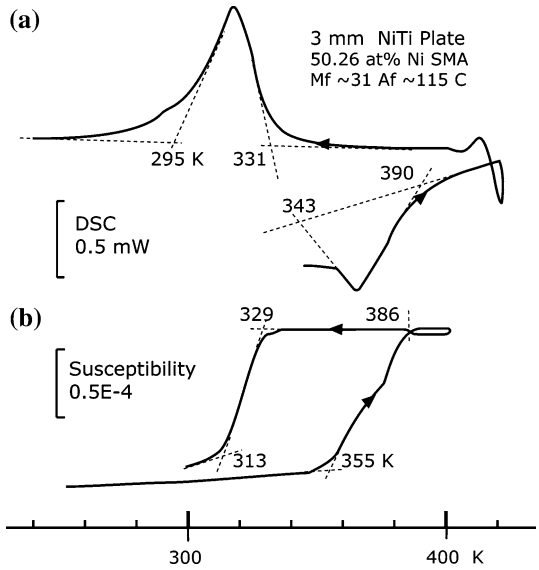

Fig. 3 **a** DSC and **b** SQUID measurements indicating transformation temperatures in a 3-mm wrought SMA plate, 50.25 at% Ni, bal. Ti

experiments designed to estimate the mechanical work energy density involved in the formation of spherical protrusions when they displace against a strong base-metal substrate under a compressive preload. In addition, we measured the maximum constrained recovery response as a function of the pre-stress level. It is shown that, by conservative estimate based on experimental determination of D^*, the energy density associated with constrained recovery in SFM is $>10^7$ J/m^3, on the order of the maximum generally available from NiTi actuators, and equal to an appreciable fraction of the experimentally determined transformational enthalpy.

Experimental methods

A 3 mm thick 50.26 at% Ni wrought NiTi alloy sheet was acquired from Special Metals Corporation. The transformation temperatures, M_f, Ms, As, and A_f, were determined by both differential scanning calorimetry (DSC) and SQUID magnetometry[2] (Fig. 3; Table 1). The enthalpy for the A to M transformation was 15.6 J/g.

Specimens were first electro-discharge cut into 12.7 mm diameter disks, ground, and polished, and finished with 0.05 μm colloidal silica. Before indenting at room temperature the specimens were briefly chilled to ensure a fully martensitic condition.

Spherical indents were made with a 1.59 mm diameter tungsten carbide ball using a load of 3000 N. Surface

[2] Squid magnetometry defines transformation temperatures somewhat more unambiguously than DSC and produces data from which M and A phase fractions may be inferred [18].

Table 1 Transformation temperatures measured by DSC and SQUID

Transformation temperature	DSC (K)	SQUID (K)	Average (K)
M_f	295	313	304 ± 9
Ms	331	329	330 ± 1
As	343	335	349 ± 6
A_f	390	386	388 ± 2

profiles of the as-indented surfaces were acquired with a WYKO NT 1000 optical surface profilometer. The initial indent depth was 240 microns and the *a/r* ratio was calculated to be 0.71. After making these measurements, and using a thermoelectric cooler (TEC) mounted on the profilometer stage, the indents were heated to 413 K (well above A_f) and profiles of the indents again recorded. Temperatures were measured by thermocouples spot-welded to the NiTi at points on either side of the indent. The specimen was then cooled to 243 K (well below M_f), using liquid Freon, to develop a fully martensitic structure. After warming to room temperature, the indents were profiled once more at 293 K, still below M_f. Fifteen $M_f \leftrightarrow A_f$ cycles were then applied to assess cyclic reversibility of the shape change. After thermal cycling, and while still in the martensitic condition, the surfaces were subjected to the planarization step, in which the specimen was flat-ground and polished, but only to the point where visible traces of the indent were removed. The final abrasive used in the planarization step was also 0.05 μm colloidal silica to minimize the effect of near-surface microstructural changes on subsequent measurements.

The constrained recovery experiments were designed to obtain an estimate of the potential work output of the SFM effect when exdented features develop during heating (Fig. 4). After planarization, the optically flat specimen was placed in contact with a base-metal coupon (also ground and polished) of 6061-T6 aluminum, or alternatively 304 and 440 SSs in certain experiments. The face-to-face pair of plates was then situated between compression platens in a servo-hydraulic load frame that was operated under load-control. At room temperature the sandwich was preloaded to various compressive stresses between 50 and 300 MPa in different experiments. After applying the preload the assembly was heated to 433 K to fully austenitize the NiTi, leading the NiTi exdent to force its way up against the constraint of the preloaded base-metal block. The depression in the base metal made in this way is referred to as a "replica" indent. After heating, and while still warm, the sandwich was first unloaded, and then cooled down to room temperature. Dimensional profiles of the NiTi and base-metal replica surfaces were subsequently acquired optically.

Figure 5 shows an optical image of the NiTi exdent (left) next to the replica indent (right) made by it in 304 SS under a pre-load of 250 MPa (the exdent was made visible by acquiring the photograph at $T > A_f$). The experiment rather clearly indicates the great force that can be exerted by SFM displacements.

There exists an alternate stress–temperature path along which the above experiment may be conducted—one that produces a more pronounced replication effect. In this variation the protocol described above is repeated, except that unloading is done *after* the specimen has cooled (i.e., cooling occurs while the servohydraulic apparatus maintained a constant axial force).

The upper limit of temperature (433 K) used in these experiments was chosen to insure full austenitization of the NiTi SFM sample under the maximum anticipated preload. Stress alters transformation temperatures according to a modified Clausius–Clapeyron equation, $dT/d\sigma = T_0\varepsilon_0/\Delta H$. The enthalpy of the SMA used in this study was 15.6 J/g, giving $dT/d\sigma = \sim 0.172$ K/MPa, such that a preload of 300 MPa would be expected to increase A_f from 388 to 440 K at the maximum preload of 300 MPa (here, T_0 is taken as $(M_f + A_f)/2$ and ε_0 is taken as 0.05, the strain at the end of the detwinning plateau). There is thus confidence that martensite was nearly fully transformed during

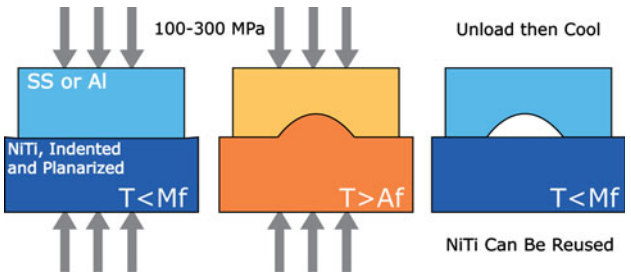

Fig. 4 Schematic illustration of the setup of the constrained recovery experiment. 304 SS is used as an example of the replica material

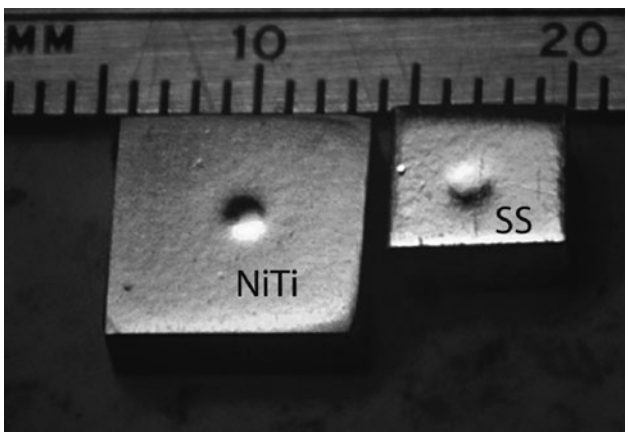

Fig. 5 Optical image of the NiTi exdent and replica indent in 304 SS after replica indentation with a preload of 250 MPa

Table 2 Calibration indentation data for 440 SS, 304 SS, and Al 6061-T6 at 433 K

Indent depth (mm)	Load (N)	Indenter radius (μm)	*a/r* ratio	Contact radius (μm)	Contact area (m^2)	Hardness, H_{440} (GPa)
440C SS						
5.0	35	800	0.112	89	2.51E − 08	1.39
7.7	55		0.138	111	3.85E − 08	1.42
12.5	100		0.176	141	6.25E − 08	1.60
					Average	1.47
304 SS						
7.9	38	800	0.140	112	3.94E − 08	0.96
11.3	56		0.167	134	5.64E − 08	0.99
19.0	105		0.217	173	9.40E − 08	1.06
					Average	1.00
6061-T6 Al						
7.5	35	800	0.137	109	3.73E − 08	0.94
11.8	55		0.171	137	5.89E − 08	0.93
23.3	103		0.240	192	11.6E − 08	0.89
					Average	0.92

heating, and the close to the maximum response was achieved.

Experiments designed to estimate the energy density connected with the displacive transformations underlying the SFM effect require that the work of indentation be estimated for a spherical indent of a given depth. This essentially amounts, in this context, to a determination of the hardness of the base metal coupons used in the study, measured using indentation geometry similar to that produced by the SFM exdent, and at a similar temperature. In addition, the hardnesses should be measured after the coupons had been cycled once to the preload stress used in the experiment (250 MPa). Measurements were made at 433 K using a 1.59 mm diameter tungsten ball under loads of 30, 50, and 100 N. The hardness values, taken as the load divided by the projected indent area, were used to interpolate the presumptive force exerted by the NiTi exdent as it displaced against the same base metal constraint, assuming that the work of indentation was the similar in both cases. Results for these calibration indentations are given in Table 2, which also gives average values that were used in the energy density calculations. To express the resulting work of indentation as an energy density we simply divided this energy by the volume of a hemisphere having radius equal to the experimentally determined value of D^* applicable to the particular *a/r* ratio used for the original NiTi indent.

Results

Spherical replica indentations

Figure 6 shows optical surface profiles for a NiTi exdent and its corresponding replica indent in 304 SS made using a preload of 250 MPa (the profile for the NiTi exdent

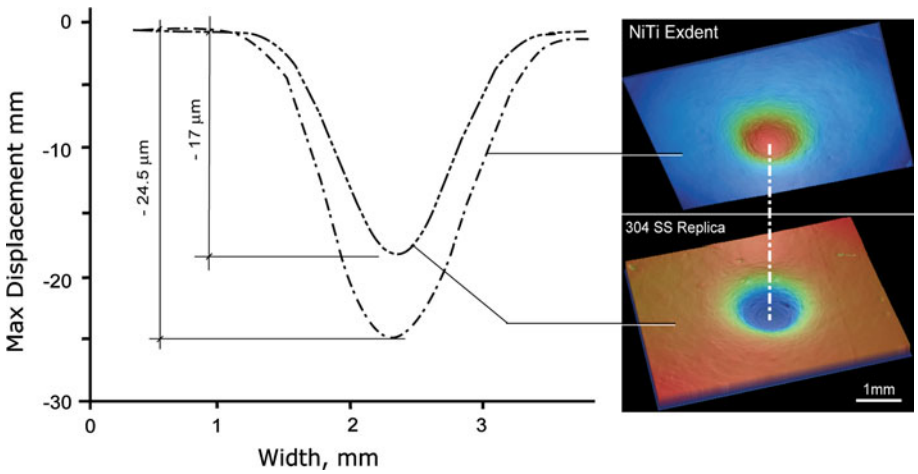

Fig. 6 Surface profiles of NiTi exdent (taken at 433 K) and a replica indent in 304 SS (taken at 293 K) for a preload of 250 MPa. The centerline profiles of the exdent and its replica indent are plotted on the *left*

having been measured at 433 K under zero load, after the replication experiment). The replica indent depth (17 μm) is around 57% of the exdent height previously measured in free recovery (30 μm). The free-recovery exdent height after the experiment decreased by 18.3% to 24.5 μm, probably because cooling under load plastically deformed the martensite at the preload stress of 250 MPa.

The relationship between the replica indent depth and the preload was determined in similar experiments for each of the three base metals. In Fig. 7, the results show that replica indent depth increases with increasing preload stress, reaching a maximum near 250 MPa, and apparently declining for higher preload stress. The peak stress level is close to the yield stress of the austenite phase in this study. Increasing the preload beyond 250 MPa leads to a drop of the replica indent depth, probably because plastic slip deformation of the NiTi during austenitization decreases the maximum NiTi exdent height, although a greater degree of work-hardening of the base metal may also contribute to the effect. It is tentatively concluded that the optimum preload stress is just below the austenite yield stress of the SMA used.

These experiments demonstrate that SFM in NiTi can be used to make replica indents in a variety of materials at various preload stresses. The hardness of the base metal naturally influences how deep a replica indent will be for a fixed preload stress. Figure 8 plots the replica indent depth against the base-metal hardness (taken as the average values reported in Table 2) for each of the three alloys, and for each of the four preload stresses used. The replica indent depth is seen to be a linear function of base-metal hardness, assuming that a base-metal hardness of zero would lead to a replica depth equal to the free-recovery height of the SFM exdent (30 microns). Extrapolation of the individual plots to zero replica indent depth provides an estimate of the maximum hardness of a base metal that could be indented by SFM for the various loads used. For example, it would be predicted that for a preload of 250 MPa, the maximum hardness, H^*, of an indentable base metal would be 2.25 GPa. Linear curve fits give H^* values of 1.87, 2.26, 2.29, and 2.63 GPa for preload stresses of 125, 200, 250, and 300 MPa, respectively, showing that H^* increases with

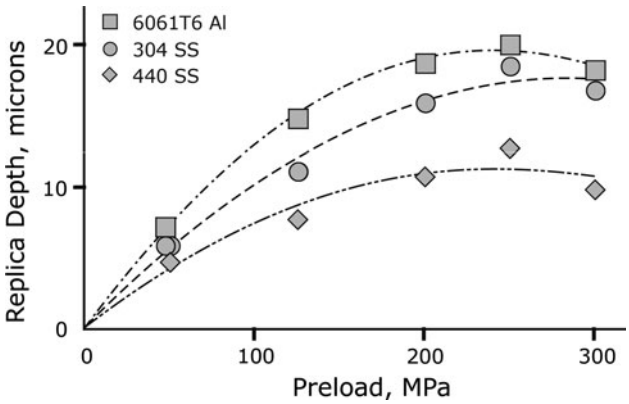

Fig. 7 The relation between replica indent depth and preload stress for two SSs and 6061-T6 aluminum (the parabolic curve fits shown were computed assuming that the replica indent depth would be zero for zero preload stress)

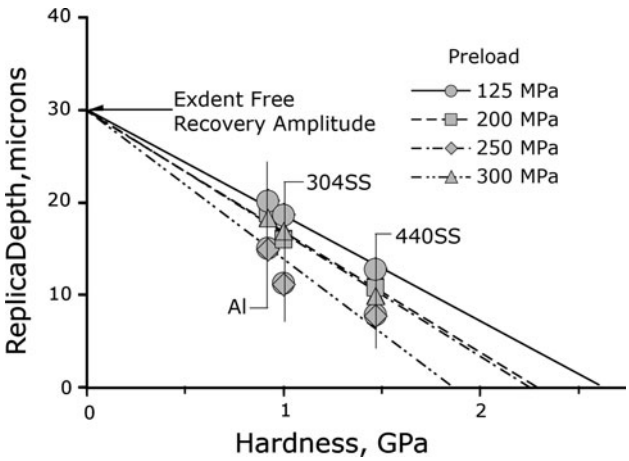

Fig. 8 Plot of replica indent depth against the material hardness at preload stresses of 125, 200, 250, and 300 MPa

increasing preload. This relationship is clearly shown in Fig. 9 which plots H^* as a function of the preload stress. A second-order polynomial fit to this data leads to a peak around 250 MPa, corresponding to the optimum preload to generate replica indent revealed in Fig. 9a. Extrapolation of the parabolic fit suggests that at a preload stress of around 480 MPa no replica indent could be made,

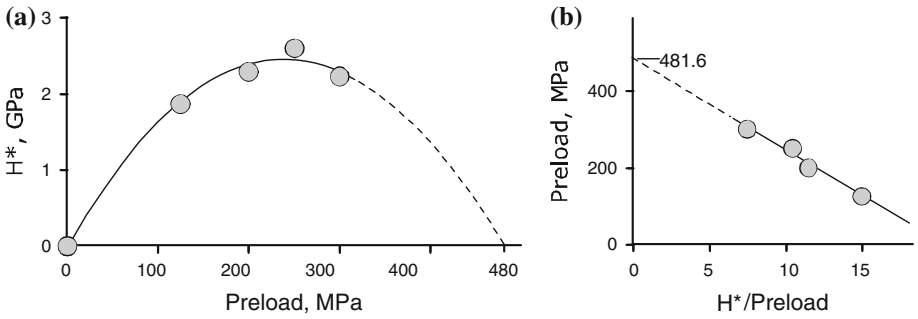

Fig. 9 **a** Plot of H^* against the preload stress. A parabolic fit suggests that 480 MPa is the largest preload stress that can be used to make a replica indent at 433 K. **b** Plotting preload stress against H^* divided by the preload produces a similar estimate

regardless of the base-metal hardness. A similar estimate comes from fitting a plot of H^* divided by the preload as a function of preload, as shown in Fig. 9b.

This maximum preload level of 480 MPa can be interpreted as a stress high enough to suppress the M-to-A transformation by increasing the transformation temperature for this reaction to above the 433 K maximum temperature used in our experiments. Assuming $dT/d\sigma = \sim 0.172$ K/MPa, as detailed in the previous section, the transformation temperatures should increase by 83 K, raising As to 432 K and A_f to 471 K. Thus, at a preload of 480 MPa, little or no transformational activity should be expected at 433 K. Conversely, if this explanation is correct, it may be possible to indent at higher preloads if the maximum temperature attained in the replication experiment were increased sufficiently. Increasing the temperature, however, will simultaneously decrease the flow stress of the austenite due to slip, and the maximum possible preload and substrate hardness levels have not yet been established.

Path dependency of replica indentation

Table 3 summarizes the effect of the unloading protocol on the replica indent depth. Data are shown for indents in 6061-T6 Al and 440 SS alloys, each processed either via path (A) in which the specimen was unloaded before cooling, or via path (B) for which cooling occurred under the preload stress of 250 MPa. The cooling rate, as measured by two thermocouples, one placed on the NiTi specimen and another placed on the replica material were in both cases approximately 5 ± 1 Ks^{-1} (the hydraulic compression stages were water cooled). For aluminum, cooling under load produced a replica that was 1.4 times deeper than occurs when cooling after unloading; for 440 SS the depth was 1.6 times greater.

Some reflection suggests that this is probably not strictly a thermomechanical path dependency, but probably relies on thermal gradients during cool-down of the specimen when processed according to path B. The exdent/replica features occupy a relatively small volume near the center of the sandwich and would thus, as shown schematically in Fig. 10, be expected to cool more slowly than material at the surfaces (where the temperature measurement was made). Therefore, as the NiTi martensitizes, it does so first at the periphery, allowing the preload stress to deform the martensite at the margins surrounding the exdent. The exdent in the interior remains austenitic longer and is thus able to further indent the base metal, up until the point when exdent also martensitizes, and therefore "retracts", some moments later. What is observed is therefore essentially an artifact of the isolated nature of the features under study, and the effect would presumably be much diminished if path B were conducted quasistatically. This conjecture is supported by the greater "path effect" seen for 440 SS (1.6× vs. 1.4× for Al). Even though the steel alloy is harder than aluminum, its lower thermal conductivity would lead to even steeper temperature gradients, magnifying the effect.

Table 3 Path dependency effect on the replica indent depth at preload of 250 MPa

Path	Replica indent depth (μm)	
	6061-Al	440 SS
A: cooling under zero load	14.3	8.0
B: cooling under 250 MPa stress	20.1	12.8
B:A ratio	1.4	1.6

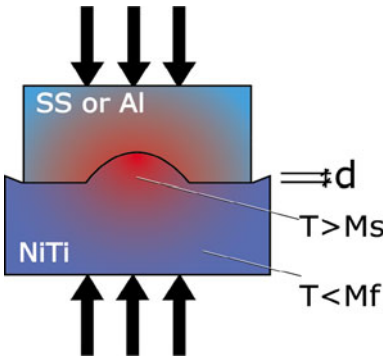

Fig. 10 Schematic temperature distribution for a NiTi–base metal couple after partial cooling from a temperature above A_f under a constant preload stress. Because the region near the exdent/replica cools more slowly there will be a period during which the material surrounding the indent has martensitized but that in the indent zone has not. The surrounding material deforms further under the constant preload stress, allowing the still-austenitic exdent to penetrate further into the base metal

Energy density calculation

Having determined the hardness, H_m (m = 6061, 304, or 440), of the base metals used in the study (see Table 2) we estimate the maximum spatially averaged force (P_{repl}) exerted by the emerging SFM exdent by multiplying H_m by the projected area of the replica indent:

$$P_{\text{repl}} = \pi a_{\text{repl}}^2 H_m$$

where a is the measured in-plane replica indent diameter. If this force increases linearly from zero to its maximum, the energy of indentation is $U_i = 1/2 P_{\text{repl}} d_{\text{repl}}$. The force–displacement curves (Fig. 11) measured by an instrumented indentation machine indicate that the load–displacement

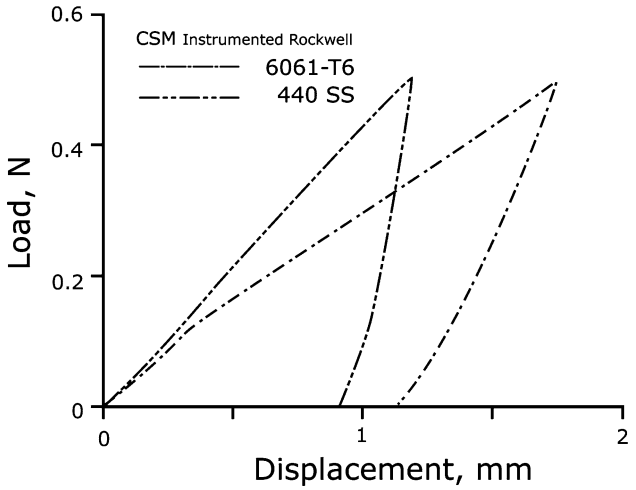

Fig. 11 Load–displacement curves of for instrumented hardness measurements on 304 SS and 6061-T6 aluminum used in the constrained recovery experiments

characteristic for indentation of 6061-T6 aluminum and 440 SS are in fact approximately linear.

To obtain the effective volumetric energy density it is necessary to make an estimate of the volume of material in which the shape-memory mechanisms occur that drive the SFM effect, i.e., the active subsurface volume contributing to formation of the exdent. We have previously determined by experiment [17] values of D^*, the depth of this zone. D^* is a function of the *a/r* ratio used to make the initial indent in the NiTi material and was found in [17] to be equal to $(1.65 \pm 0.09)a$ for an *a/r* ratio of 0.71.

With a simplifying assumption that D^* represents the radius of a hemispherical "active zone" centered on base of the indent, we estimate the volume of the active zone as $V^* = 1/2\ (4/3\pi D^{*3})$. Dividing the energy of indentation, U_i, by this quantity then provides an estimate of the volumetric energy density associated with exdent formation in NiTi during a constrained recovery SFM event. Results of this calculation for the three base metals studied are summarized in Table 4. Energy densities estimated in this way have an average about 12 MJ/m^3 for the three materials at 250 MPa preload.

Conclusions

Indentation of martensitic NiTi alloy to a depth such that the *a/r* ratio exceeds about 0.25 leads to two-way shape memory displacements causing the indent to be shallow when hot and deeper when cool. When such an indent is ground away at $T < M_f$, a bump, or "exdent" will appear at the site of the indentation that can be caused to emerge and retreat on thermal cycling between M_f and A_f. The present experiments show that these surface form memory displacements can exert sufficient force to plastically deform a strong base metal alloy, creating what we call a replica indent. A single SFM exdent can repeatedly create replica indents in 440 SS with the depth declining over the first few thermal cycles. It was found that the maximum shape recovery response occurred when a preload of 250 MPa was used. Minimal shape recovery response occurred at the preload of around 480 MPa, a stress sufficient to inhibit martensite-to-austenite transformation. The replica indent depth could also be increased by cooling under load.

Preliminary experiments on low cycle fatigue test of cyclically stable exdents indicate that the replica indent depth stabilizes after a number of repeated replica indentations for different preload conditions due to the balance between work hardening and plastic deformation of NiTi exdent. In view of the fact that the process operates robustly at the nanoscale, the new technique may be applicable to a wide range of engineering problems from MEMS microassembly to nanolithography to thermally variable friction surfaces.

Table 4 Calculation of energy density for replica indent made under 250 MPa

Material	Indent depth (m)	Replica contact radius a_{repl} (m)	Replica *a/r* ratio	Replica contact area, A_{repl} (m^2)	Equivalent replicant load, P_{repl} (N)	Indentation energy, U (J)	Est. D^* (m)	Est. energy density (MJ/m^3)
440 SS	12.8	868.71	0.0295	2.37	3.49	2.23	0.94	**12.8**
	E − 06	E − 06		E − 06	E + 03	E − 02	E − 03	
304 SS	18.6	837.69	0.0444	2.20	2.20	2.05	0.94	**11.8**
	E − 06	E − 06		E − 06	E + 03	E − 02	E − 03	
6061 Al	20.1	832.71	0.0482	2.18	2.00	2.01	0.94	**11.6**
	E − 06	E − 06		E − 06	E + 03	E − 02	E − 03	

Boldface indicates the most important data

Acknowledgements The authors gratefully acknowledge funding from the National Science Foundation under grants CMS0336810 and CMS0510294, and from General Motors Corporation.

References

1. Chau ETF, Friend CM, Allen DM, Hora J, Webster JR (2006) Mater Sci Eng A 438:589
2. Gil FJ, Planell JA (1998) Proc Inst Mech Eng 212:473
3. Besselink PA, Sachdeva RCL (1995) J De Phys IV 5:C8
4. Predki W, Knopik A, Bauer B (2008) Mater Sci Eng A 481:598
5. Mertmann M (2004) Minim Invasive Ther Allied Technol 13:254
6. Wolf RH, Heuer AH (1995) J Microelectromech Syst 4:1057
7. Lahoz R, Gracia-Villa L, Puertolas JA (2002) J Eng Mater Technol Trans Asme 124:397
8. Perkins J, Sponholz RO (1984) Metall Trans 15A:313
9. Yu HJ (2006) J Mater Sci 41:3435. doi:10.1007/s10853-005-5908-6
10. Zhang YJ, Cheng YT, Grummon DS (2006) Appl Phys Lett 89:1912
11. Zhang YJ, Cheng YT, Grummon DS (2006) Appl Phys Lett 88:1904
12. Fei XL (2011) Ph.D Dissertation, Michigan State University, East Lansing
13. Ni WY, Cheng YT, Grummon DS (2003) Appl Phys Lett 82:2811
14. Tabor D (1948) Proc Royal Soc Lond Ser A Math Phys Sci 192:247
15. Tabor D (1996) Philos Mag A Phys Condens Matter Struct Defects Mech Prop 74:1207
16. Zhang YJ, Cheng YT, Grummon DS (2007) J Mater Res 22:2851
17. Fei XL, Zhang YJ, Grummon DS, Cheng YT (2009) J Mater Res 24:823
18. Pence TJ, Wu X, Grummon DS (1999) Mater Sci Eng A 273–275:722